UTMS 2009–20 September 17, 2009

Numerical simulations of two-dimensional fractional subdiffusion problems

by

Hermann Brunner, Leevan Ling
and Masahiro Yamamoto

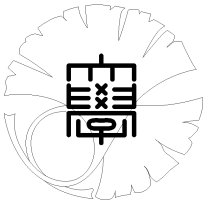

UNIVERSITY OF TOKYO
GRADUATE SCHOOL OF MATHEMATICAL SCIENCES
KOMABA, TOKYO, JAPAN

Numerical simulations of two-dimensional fractional subdiffusion problems

Hermann Brunner*, Leevan Ling† and Masahiro Yamamoto ‡

Abstract

The growing number of applications of fractional derivatives in various fields of science and engineering indicates that there is a significant demand for better mathematical algorithms for models with real objects and processes. Currently, most algorithms are designed for 1D problems due to the memory effect in fractional derivatives. In this work, the 2D fractional subdiffusion problems are solved by an algorithm that couples an adaptive time stepping and adaptive spatial basis selection approach. The proposed algorithm is also used to simulate a subdiffusion-convection equation.

1 Introduction

Let Ω be a bounded domain in $\mathbb{R}^2$ with sufficiently smooth boundary $\partial\Omega = \Gamma_D \cup \Gamma_N$ with $\Gamma_D \cap \Gamma_N = \emptyset$. We consider an initial-boundary problem for a time fractional diffusion equation with fractional-order $0 < \alpha < 1$:

$$\begin{aligned} {}^cD_t^\alpha u(x,t) &= \Delta u(x,t) + f(x), && x \in \Omega, \quad t \in (0,T), \\ u(x,0) &= u_0(x), && x \in \Omega, \\ u(x,t) &= g_0(x,t), && x \in \Gamma_D, \quad t \in (0,T), \\ \partial_\nu u(x,t) &= g_1(x,t), && x \in \Gamma_N \quad t \in (0,T), \end{aligned} \tag{1}$$

Preliminary Draft — File: fracdiffusion04.tex *— Not For Distribution.*

*Department of Mathematics, Hong Kong Baptist University, Kowloon Tong, Hong Kong. (E-mail: hbrunner@math.hkbu.edu.hk)

†Department of Mathematics, Hong Kong Baptist University, Kowloon Tong, Hong Kong. (E-mail: lling@hkbu.edu.hk)

‡Graduate School of Mathematical Sciences, University of Tokyo, 3-8-1 Komaba Meguro Tokyo 153 (E-mail: myama@ms.u-tokyo.ac.jp)

Key words and phrases. Kansa's method, adaptive greedy algorithm, geometric time grids

where ${}^cD_t^\alpha$ denotes the Caputo fractional derivative of order α with respect to t defined by

$$ {}^cD_t^\alpha u(x,t) = \frac{1}{\Gamma(1-\alpha)} \int_0^t \frac{\partial u(x,\eta)}{\partial \eta} \frac{d\eta}{(t-\eta)^\alpha}, \quad 0 < \alpha < 1, \tag{2} $$

see monograph by Podlubny [22]. The operator Δ is the Laplacian in $\mathbb{R}^2$ and ∂_ν is the outward normal derivative. Note that if $\alpha = 1$, then the Caputo fractional derivative in (2) becomes $\partial_t u(x,t)$ and the problem in (1) represents the standard integer-order parabolic equation.

The fractional diffusion equation is related with the continuous-time random walk and is a model for anomalous diffusion in many applied fields such as diffusion processes of contaminants in porous media, see [8, 9, 17, 18] and the references therein.

In this paper, we discuss a numerical algorithm that couples an adaptive time stepping and an adaptive spatial basis selection approach, and show numerical results.

As for works on numerical methods for fractional diffusion equations appearing in (1.1), we can refer to [1, 4, 5, 6, 11, 19, 20, 21, 23, 24, 26, 27]. Among the above works, except for [27], all the papers treat the case where the spatial dimension is one; see also [21] for a nonlinear fractional diffusion equation. As for available numerical methods for fractional diffusion equations, see [7] and [25].

2 Methodology

2.1 Finite difference time discretization

We employ the difference approximation in [16] for the fractional time derivative. Suppose the time interval $[0, T]$ is discretized uniformly into n subintervals; define $t_k = k \cdot \triangle t$, $k = 0, 1, \ldots, K$, where $\triangle t = T/n$ is the time step. Let $\lambda(t_k)$ be the exact value of a function $\lambda(t)$ at time step t_k. Then, the fractional time derivative can be approximated by the following scheme:

$$
\begin{aligned}
{}^cD_t^\alpha \lambda(t_{k+1}) &= \frac{1}{\Gamma(1-\alpha)} \int_0^t \frac{\partial \lambda(t)}{\partial \eta} \frac{d\eta}{(t-\eta)^\alpha} \\
&\approx \frac{1}{\Gamma(1-\alpha)} \sum_{j=0}^{k} \frac{\lambda(t_{j+1}) - \lambda(t_j)}{\triangle t} \int_{j\triangle t}^{(j+1)\triangle t} \frac{d\eta}{(t_{k+1}-\eta)^\alpha} \\
&= \frac{1}{\Gamma(1-\alpha)} \sum_{j=0}^{k} \frac{\lambda(t_{j+1}) - \lambda(t_j)}{\triangle t} \int_{(k-j+1)\triangle t}^{(k-j)\triangle t} \eta^{-\alpha} d\eta \\
&= \frac{1}{\Gamma(1-\alpha)} \sum_{j=0}^{k} \frac{\lambda(t_{k+1-j}) - \lambda(t_{k-j})}{\triangle t} \int_{j\triangle t}^{(j+1)\triangle t} \eta^{-\alpha} d\eta \\
&= \frac{(\triangle t)^{1-\alpha}}{\Gamma(2-\alpha)} \sum_{j=0}^{k} \frac{\lambda(t_{k+1-j}) - \lambda(t_{k-j})}{\triangle t} \big[(j+1)^{1-\alpha} - j^{1-\alpha}\big].
\end{aligned}
$$

Hence, we obtain a first-order discretization

$$
{}^cD_t^\alpha \lambda(t_{k+1}) \approx {}^c\triangle_t^\alpha \lambda(t_{k+1}) := \frac{(\triangle t)^{-\alpha}}{\Gamma(2-\alpha)} \sum_{j=0}^{k} w_j \big[\lambda(t_{k+1-j}) - \lambda(t_{k-j})\big], \quad (3)
$$

for $k = 0, \ldots, K-1$ where the weight is defined as $w_j = [(j+1)^{1-\alpha} - j^{1-\alpha}]$ for $j = 0, 1, \ldots, K$. Equation (3) can be easily rewritten to obtain a fully explicit scheme for the latest approximation $\lambda(t_{k+1})$ which depends on all previous values $\lambda(t_0), \ldots, \lambda(t_k)$.

2.2 Kernel based spatial approximation

In this section, we consider a kernel-basis representation for the spatial variables. For the considered problem (1), the numerical approximation is expanded as

$$
u(x,t) \approx U(x,t) = \sum_{\ell=1}^{N} \lambda_\ell(t) \Phi\big(\|x - \xi_\ell\|/c\big), \quad x \in \Omega, \quad (4)
$$

where c is the scaling parameter, the set $\Xi = \{\xi_\ell\}_{\ell=1}^N$ is the trial centers and $\Phi(\cdot)$ can be any commonly used radial basis kernel; for examples, multiquadrics $\Phi(r) = (r+1)^{1/2}$, inverse multiquadrics $\Phi(r) = (r+1)^{-1/2}$, gaussian $\Phi(r) = \exp(-r^2)$, thin plate spline $\Phi(r) = r^2 \log(r)$, etc. Putting (4) into the subdiffusion equation (1) results in

$$
\sum_{\ell=1}^{N} {}^cD_t^\alpha \lambda_\ell(t) \Phi\big(\|x - \xi_\ell\|/c\big) = \sum_{\ell=1}^{N} \lambda_\ell(t) \Delta\Phi\big(\|x - \xi_\ell\|/c\big) + f(x). \quad (5)
$$

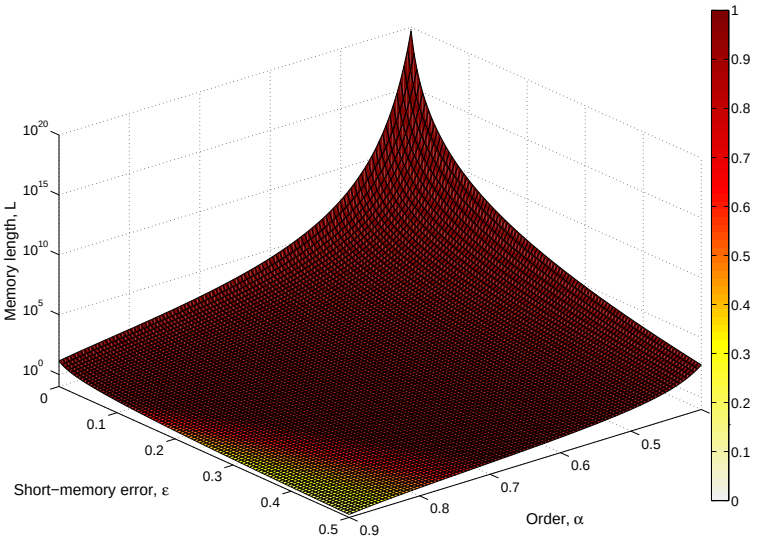

Figure 1: Memory length L required for various orders α and desired accuracy ϵ in the "short-memory" principle.

Using a sufficiently dense set $X = \{x_1, x_2, \ldots, x_M\} \subset \bar{\Omega}$ for collocation, applying the finite difference ${}^c\triangle_t^\alpha$ in (3) to $\lambda_\ell(\cdot)$ and the strong form collocations at X will result in a matrix system for updating (discrete) values of the coefficient functions $\lambda_\ell(t_k)$, $\ell = 1, \ldots, N$, $k = 1, \ldots, K$.

2.3 Geometric time grids

When $t \gg 0$, the size of "memory" in the fractional-derivative approximation becomes enormously large. The "short-memory" principle suggests that, for large t, the role of the "history" of the behavior of the solution $u(x,t)$ near $t = 0$ can be neglected. This agrees with the fact that $w_j \searrow 0$ in (3) as $j \nearrow$ with large n. Hence, one may take into account the behavior of $u(x,t)$ in the recent past in the interval $[t - L,\, t]$ where L is the "memory length". It is shown [22, Ch.7] that

$$| \, {}^cD_t^\alpha \lambda(t) - \, {}_{t-L}{}^cD_t^\alpha \lambda(t)| \le \epsilon, \quad \text{if } L \ge \left(\frac{M}{\epsilon |\Gamma(1-\alpha)|} \right)^{1/\alpha},$$

where ${}_{t-L}{}^cD_t^\alpha$ is the fractional derivative with moving lower integration limit $t - L$ in the definition (2), instead of 0.

Despite of its success in 1D problems, Figure 1 shows that the short-memory principle is not particularly useful in reducing the memory requirement in 2D when $t \approx 1$. The penalty in the form of inaccuracy is too large; for example, when $\alpha = 0.5$, any memory length $L < 1$ will introduce an error $\epsilon \gg 1$. As we will see soon in the numerical experiment, small time stepping is important to capture the fast "initial drop" [22, Ch.3] accurately. Hence, we turn our focus to the *geometric time grids* [2, 3].

For large t away from 0, the solutions of subdiffusion "diffuse slower" than the standard integer-order diffusion process. It makes sense to employ a large time step in this region. Let $U(\cdot, t_k)$ be the numerical approximation for $u(\cdot, t_k)$. To monitor this diffusion rate, we define a measure between the numerical solutions $U(x, \cdot)$ of two consecutive time steps by

$$\Delta U_{t_k} = \frac{\|U(x, t_k) - U(x, t_{k-1})\|_{L^2(\Omega)}}{\|U(x, t_{k-1})\|_{L^2(\Omega)}}, \quad \text{for} \quad k = 1, \ldots, K. \tag{6}$$

For some user-defined relaxation parameters τ, if $\Delta U_{t_i} < \tau$, the time spacing is relaxed:

$$\triangle t \leftarrow 2 \cdot \triangle t,$$

up to some prefixed value $\triangle t_{\max}$.

2.4 Adaptive kernel selections

Although the geometric time grids can help reduce the number of previous solutions needed for evaluating ${}^c\triangle_t^\alpha u(x, t)$ at current time, it is not possible to completely remove the memory nature as it comes directly from the fractional subdiffusion problem. To effectively minimize the overhead of computer memory, the spatial information must be carefully treated. Using kernel representation, a kind of meshless method, expansion (4) provides us a parametric description of the numerical approximation. This is the first motivation of employing an adaptive technique so that only a small subset of $\lambda_\ell(t_k)$ are stored instead of all approximation values $U(X, t_k)$.

However, kernel representation is not at all trouble-free. For example, choosing trial centers Ξ is a common problem for researchers who employ various meshless methods. On one hand, high accuracy is always desired; on the other, ill-conditioning problems of the resultant matrices, that may lead to unstable algorithms, prevent some researchers from using meshless methods. For example, the optimal placements of source points in the method of fundamental solutions, or of the centers in the radial basis functions method are always unclear. Intuitively, such optimal locations will depend on many factors: the partial differential equations, the domain, the trial basis used (i.e.

the employed method itself), the computational precisions, some user-defined parameters, and so on. Such complexity makes the hope of having optimal trial centers placement unpromising. Our previous papers [12, 13, 14, 15] are devoted on the sub-optimal solution to the placement problem. In particular, we employ the most up-to-date algorithm in [15]. The first assumption is that $|\Xi| \geq |X|$ so that there are more than the necessary number of basis functions in (4) and, by applying the adaptive algorithm, the "proper" subset of Ξ will be selected. Before describing the algorithm, we emphasize the algorithm presented below is matrix-free in the sense that resultant matrix will not be fully evaluated or stored. Hence, the increase in number of basis functions does not impose an overhead to the memory requirement; that is one of the main concerns in solving fractional subdiffusion equations.

Without going into the how-and-why, we present the key steps of the adaptive algorithm in [15]. Readers can refer to the original article for details. Consider any matrix system with $A \in \mathbb{R}^{M\times N}$ and $b \in \mathbb{R}^M$ usually with $M \leq N$. Moreover, we denote submatrices of A by $A(\,\cdot\,,\,\cdot\,) : (\mathbb{R}^d)^m \times (\mathbb{R}^d)^n \to \mathbb{R}^{m\times n}$ as a matrix function taking sets of collocation points and sets of RBF centers, respectively, as first and second input arguments. Similarly, the right-hand vector $b(\,\cdot\,) : (\mathbb{R}^d)^m \to \mathbb{R}^m$ can be treated as a vector function that can be specified by the collocations points. For example, $A = A(X_M, \Xi_N) \in \mathbb{R}^{M\times N}$ and $b = b(X_M) \in \mathbb{R}^M$ are, respectively, the original matrix and the right-hand vector.

The adaptive algorithm will build, for $A\lambda = b$, an ordered indexed sets, denoted by $X_{(k)} = \{x_{(1)}, \ldots, x_{(k)}\}$ and $\Xi_{(k)} = \{\xi_{(1)}, \ldots, \xi_{(k)}\}$, for $k = 1, \ldots, M$, for collocation points and trial centers respectively. Suppose, after k iterations, our algorithm selects a set of k collocation points $X_{(k)} \subset X$ and a set k RBF centers $\Xi_{(k)} \subset \Xi$, respectively. These sets of points define a subproblem to the original one:

$$\begin{cases} A_{(k)}\check{\lambda}^{(k)} = \check{b}^{(k)}, \\ A_{(k)}^T\check{\nu}^{(k)} = -\check{\lambda}^{(k)}, \end{cases} \tag{7}$$

where $A_{(k)} = A(X_{(k)}, \Xi_{(k)}) \in \mathbb{R}^{k\times k}$ is a square submatrix of the full matrix A and $\check{b}^{(k)} = b(X_{(k)}) \in \mathbb{R}^k$. After solving (7) for $\check{\lambda}^{(k)} \in \mathbb{R}^k$, let $\lambda^{(k)} \in \mathbb{R}^N$ be the extension of $\check{\lambda}^{(k)}$ by patching zeros into entries associated with the non-selected RBF centers. Similarly, $\check{\nu}^{(k)} \in \mathbb{R}^k$ can be extended to $\nu^{(k)} \in \mathbb{R}^N$.

The $(k+1)^{\text{st}}$ collocation point $x_{(k+1)}$ and RBF center $\xi_{(k+1)}$ can be selected from the primal residual

$$r^{(k)} = A\lambda^{(k)} - b = A(X_M, \Xi_{(k)})\check{\lambda}^{(k)} - b. \tag{8}$$

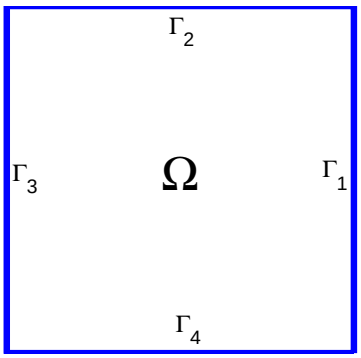

Figure 2: Boundary labels for $\Omega = [-1, 1]^2$.

and the dual residual

$$q^{(k)} = \lambda^{(k)} + A^T \nu^{(k)} = \lambda^{(k)} + [A(X_{(k)}, \Xi_N)]^T \check{\nu}^{(k)}. \tag{9}$$

respectively, using the *greedy* technique. We pick from the set of collocation points X_M a collocation point $x_{(k+1)}$ such that the corresponding entry in the primal residual $r^{(k)}$ is the largest in absolute value. Similarly, the new RBF center $\xi_{(k+1)}$ is selected from all candidates in Ξ_N such that $q^{(k)}$ is the largest in absolute value among all others.

3 Numerical verifications for $\alpha = \frac{1}{2}$

For the sake of error analysis, the existence of a unique exact solution is desired. We verify the proposed numerical scheme to solve a simplified problem with zero Dirichlet/Neumann/mized boundary conditions:

$$\begin{array}{rcllll} {}^cD_t^\alpha u(x,t) & = & \Delta u(x,t), & x \in \Omega, & t \in (0,T), & 0 < \alpha < 1, \\ u(x,0) & = & u_0(x), & x \in \Omega, & & \\ u(x,t) & = & 0, & x \in \Gamma_D, & t \in (0,T), & \\ \partial_\nu u(x,t) & = & 0, & x \in \Gamma_N & t \in (0,T). & \end{array} \tag{10}$$

Let $\Omega = [-1, 1]^2$ whose boundaries are labeled as in Figure 2. We consider three cases:

Dirichlet BC is imposed on the whole boundary $\Gamma_D = \partial\Omega$. Using the fact that

$${}^cD_t^{\frac{1}{2}} \operatorname{erfcx}(\lambda t) = -\lambda \operatorname{erfcx}(\lambda t),$$

the exact solution of (10) associated with initial condition

$$u_0(x) = \cos\left(\frac{\pi}{2}x\right)\cos\left(\frac{\pi}{2}y\right)$$

is given as

$$w_1(x,t) = \text{erfcx}\left(\frac{1}{2}\pi^2 t^\alpha\right)\cos\left(\frac{\pi}{2}x\right)\cos\left(\frac{\pi}{2}y\right),$$

where *erfcx* is the *scaled complementary error function* defined by

$$\text{erfcx}(z) = \frac{2}{\sqrt{\pi}}\exp(z^2)\int_z^\infty \exp(-\eta^2)\,d\eta.$$

Neumann BC: is imposed on the whole boundary $\Gamma_N = \partial\Omega$ with initial condition

$$u_0(x) = \sin\left(\frac{\pi}{2}x\right)\sin\left(\frac{\pi}{2}y\right).$$

The exact solution is $\text{erfcx}\left(\frac{1}{2}\pi^2 t^\alpha\right) u_0(x)$.

Mixed BC: with Dirichlet BC on $\Gamma_D = \Gamma_1 \cup \Gamma_3$ and Neumann BC on $\Gamma_N = \Gamma_2 \cup \Gamma_4$. Initial condition is

$$u_0(x) = \cos\left(\frac{\pi}{2}x\right)\sin\left(\frac{\pi}{2}y\right).$$

Similarly, the exact solution is $\text{erfcx}\left(\frac{1}{2}\pi^2 t^\alpha\right) u_0(x)$.

A total number of 1537 trial basis functions, including both interior and boundary nodes, is fed into the adaptive algorithm for all time. For all three boundary conditions and all time updates, the numbers of selected basis range between 82 to 146 that is an over 90% saving in memory requirement. The initial time step is $dt = 2^{-13}$ and it is relaxed whenever the measure in (6) is less than $\tau = 0\%$, 0.5%, 1.0%, and 10%. When $\tau = 0\%$, the time stepping is fixed at $dt = 2^{-13}$ for all time. Figure 3 to Figure 4 show the absolute and relative errors over $t = (0, 1]$.

One interesting observation (see Figure 3 and Figure 4) is that fine time stepping ($\tau = 0\%$) does not result in the best accuracy due to the presence of cancelation errors. When τ is large, e.g. 10%, the time spacing is relaxed too early and hence thus results in poor accuracy near $t = 0$. However, as t increases, we see that the numerical solutions for $\tau = 10\%$ is more accurate than those for $\tau = 0\%$. This tells how severe the cancelation errors are. Better results can be obtained by small tolerances $\tau = 0.5\%$ or 1.0%. Note that using small $\tau > 0$ requires more (but still much faster than using fixed small time step) computational time.

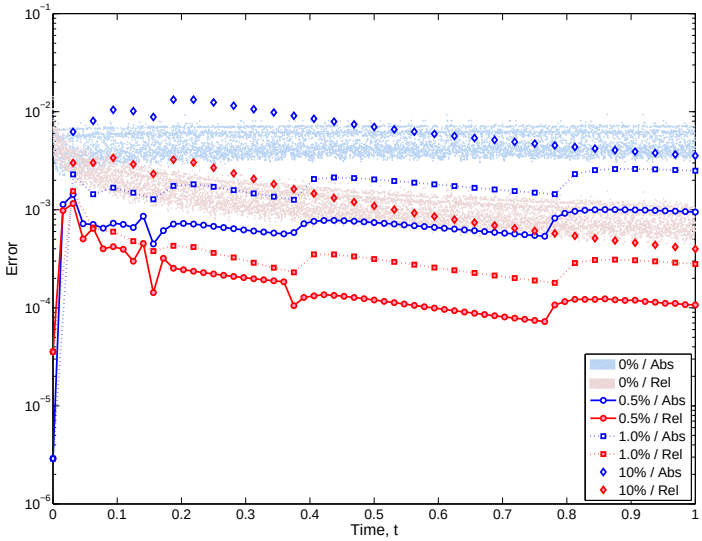

Figure 3: Dirichlet boundary conditions: Absolute and relative errors over time for different relaxation parameters $\tau = 0\%$, 0.5%, 1.0%, and 10%.

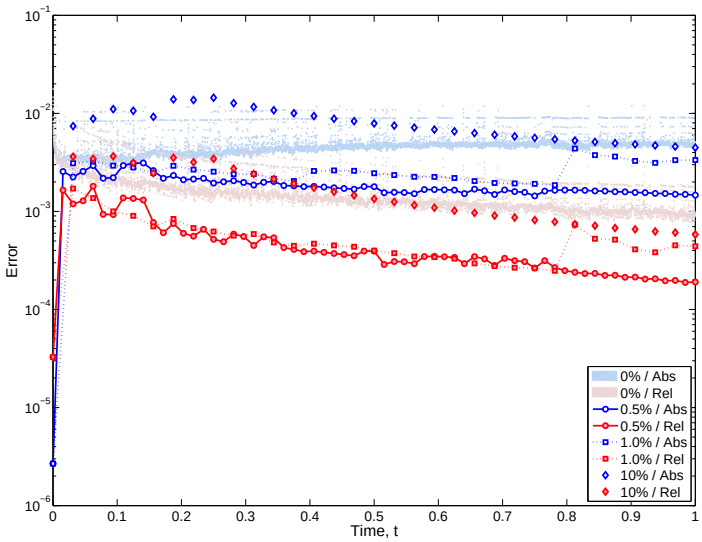

Figure 4: Neumann boundary conditions: Absolute and relative errors over time for different relaxation parameters $\tau = 0\%$, 0.5%, 1.0%, and 10%.

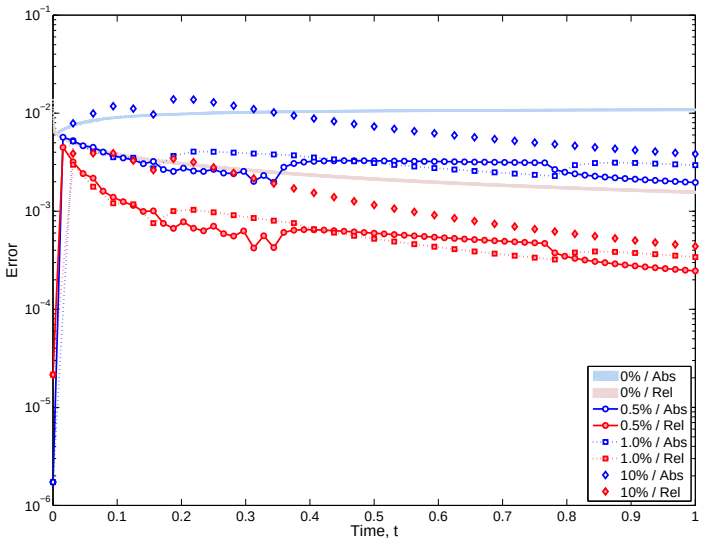

Figure 5: Mixed boundary conditions: Absolute and relative errors over time for different relaxation parameters $\tau = 0\%$, 0.5%, 1.0%, and 10%.

4 Numerical simulations

Our first simulation studies the effect of the order α on the decay rate of the subdiffusion solution. We consider (10) with Neumann boundary condition for insulated boundary. Initial time stepping is $dt = 2^{-13}$ and the relaxation parameter is set to be $\tau = 0.05\%$. Figure 6 shows the maximum norm of the numerical solution for $\alpha = 0.1, 0.2, \ldots, 0.9$ and time $t \in [0, 1]$; the dots in Figure 6 indicate all visited times in each run. For small α, say 0.1, the initial drop is enormous; in case of $\alpha = 0.1$, the maximum norm of the solution immediately drops from 1 to 0.34 after the first time update. On the other hand, when time gets large, the change in the solution is relatively minor; dt is relaxed all the way to $dt_{\max} = 2^{-5}$. For large α, the solution behaves more like the integer-order case. When $\alpha = 0.9$, the largest time stepping used is $dt = 2^{-8}$. In the experiment, we see that a very small initial time stepping is desired for small α. Whereas, when α is large, a more easygoing relaxation scheme is desired.

Our last example simulates the fractional subdiffusion-convection prob-

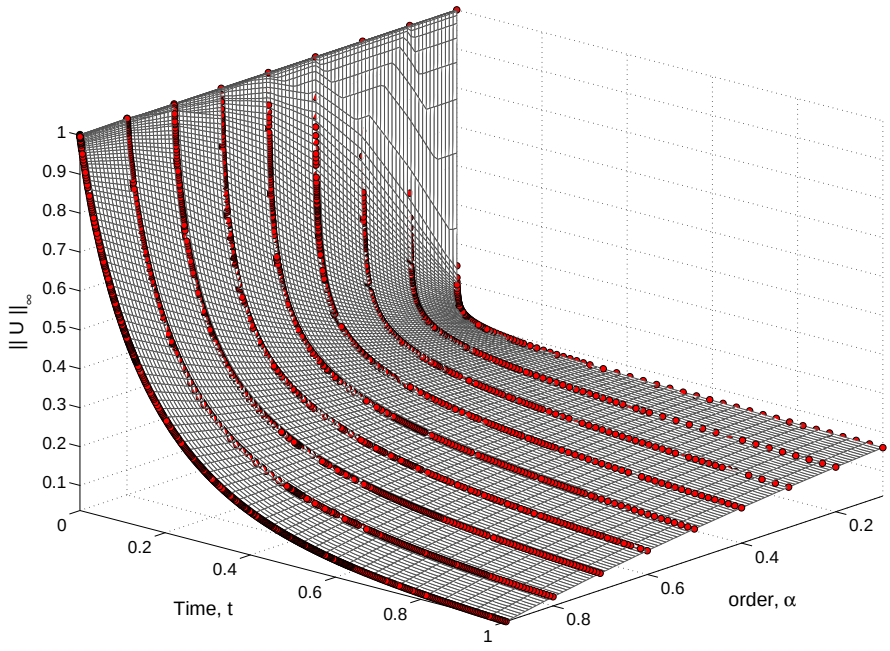

Figure 6: Maximum norm of numerical solution to the subdiffusion problem (10) with Neumann boundary conditions for $\alpha = 0.1, 0.2, \ldots, 0.9$.

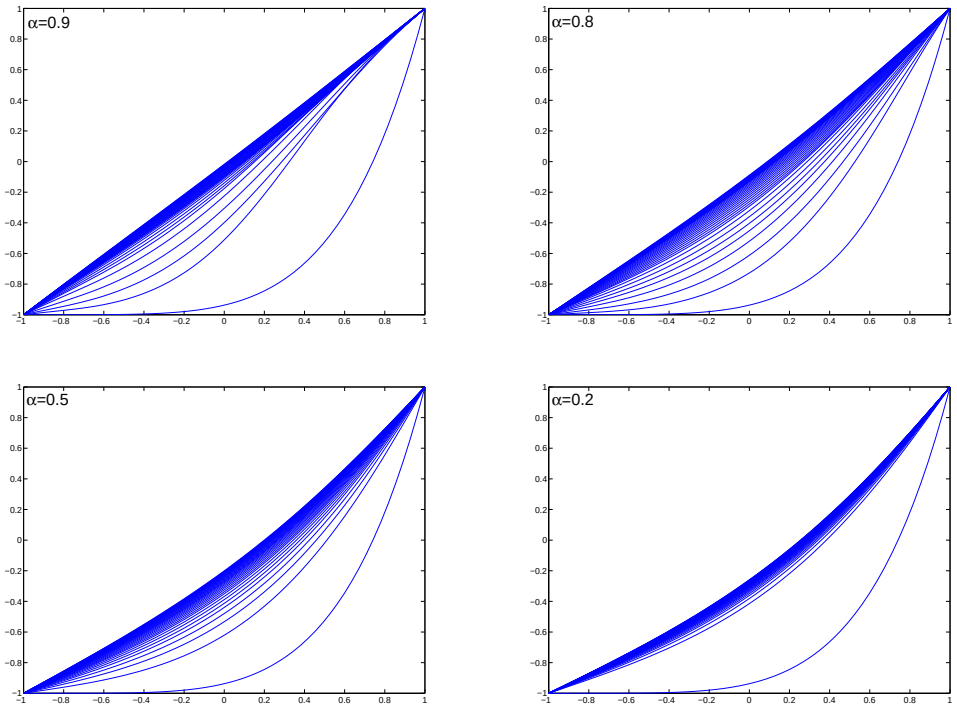

Figure 7: Numerical solution (cross section) for a fractional subdiffusion-convection problem with different α.

lem,

$$\begin{aligned} {}^{c}D_t^{\alpha} u(x,t) &= \Delta u(x,t) + \omega \frac{\partial}{\partial x} u(x,t), && x \in \Omega, \\ u(x,0) &= 2\left(\frac{x_1+1}{2}\right)^5 - 1, && x = (x_1, x_2) \in \Omega, \\ u(x,t) &= x_1, && x \in \Gamma_1 \cup \Gamma_3, \\ \partial_\nu u(x,t) &= 0, && x \in \Gamma_2 \cup \Gamma_4 \end{aligned}$$

for $\alpha = \{0.9, 0.8, 0.5, 0.2\}$, $t \in (0,1)$ and $\omega = 0.005$ is the convection coefficient. Due to the symmetry of the problem, we show the cross section of the numerical solution (parallel to the x_1-axis) in Figure 7 for every $1/32$ sec moving up from the lower-right towards the diagonal.

The effect of convection can be seen most clearly in the case of $\alpha = 0.9$; the presence of the points of inflection is obvious for small t. The effect of convection is less clear as α decreases. After careful examination, one may still find some inflection points for the case of $\alpha = 0.8$. However, when

$\alpha = 0.5$, the effect of convection becomes even less significant. For $\alpha = 0.2$, as in the previous example, we see a very rapid change in the solution between $(0, \epsilon)$; after that, the solution varies slowly. Note also that the numerical solutions for different α are more distinct near the left endpoint where fluid is being pumped out. For experiment design, it makes sense to place sensors somewhere in $-1 < x_1 < 0$ instead of in $0 < x_1 < 1$.

5 Conclusion

We present a numerical scheme, which includes geometric time grids relaxation and adaptive kernel selection, for solving the 2D fraction subdiffusion problems. The algorithm is tested with different boundary conditions, for which exact solutions are known, in order to verify its accuracy. Next, the algorithm is applied to simulate the subdiffusion problems with different fractional-orders and a subdiffusion-convection problem.

Since the kernel presentation is used for spatial discretization, implicitly, we required the initial condition to be of certainly smoothness. In cases that is not true, one should employ finite element or finite difference scheme for the first few time steps. Once the numerical solution (sub)diffuses and becomes smooth, the kernel presentation can be re-introduced. The memory saving provided by the adaptive kernel selection will become more significant in 3D. The simulations in [10] suggest that the adaptive algorithm takes roughly about 500 trial basis for approximating smooth functions in $[-1, 1]^3$. This suggests that the proposed algorithm has a good chance in solving 3D subdiffusion problems without modification. We leave this to our future studies.

Acknowledgements

This project was supported by the CERG Grant of Hong Kong Research Grant Council and the FRG grant of Hong Kong Baptist University. This work has been mostly done during the stay of the second named author at the Graduate School of Mathematical Sciences of the University of Tokyo in December 2008–January 2009, and the stay was supported by Global COE Program "The Research and Training Center for New Development in Mathematics."

References

[1] K. Al-Khaled and S. Momani. An approximate solution for a fractional diffusion-wave equation using the decomposition method. *Appl. Math. Comput.*, 165(2):473–483, 2005.

[2] H. Brunner. *Collocation methods for Volterra integral and related functional differential equations*, volume 15 of *Cambridge Monographs on Applied and Computational Mathematics*. Cambridge University Press, Cambridge, 2004.

[3] H. Brunner, A. Pedas, and G. Vainikko. Piecewise polynomial collocation methods for linear Volterra integro-differential equations with weakly singular kernels. *SIAM J. Numer. Anal.*, 39(3):957–982, 2001.

[4] E. Cuesta, C. Lubich, and C. Palencia. Convolution quadrature time discretization of fractional diffusion-wave equations. *Math. Comp.*, 75(254):673–696, 2006.

[5] E. Cuesta and C. Palencia. A numerical method for an integro-differential equation with memory in Banach spaces: qualitative properties. *SIAM J. Numer. Anal.*, 41(4):1232–1241, 2003.

[6] W. Deng. Numerical algorithm for the time fractional Fokker-Planck equation. *J. Comput. Phys.*, 227(2):1510–1522, 2007.

[7] K. Diethelm, N. J. Ford, A. D. Freed, and Y. Luchko. Algorithms for the fractional calculus: a selection of numerical methods. *Comput. Methods Appl. Mech. Engrg.*, 194(6-8):743–773, 2005.

[8] R. Gorenflo, F. Mainardi, D. Moretti, and P. Paradisi. Time fractional diffusion: a discrete random walk approach. *Nonlinear Dynam.*, 29(1-4):129–143, 2002.

[9] R. Gorenflo, F. Mainardi, and A. Vivoli. Continuous-time random walk and parametric subordination in fractional diffusion. *Chaos Solitons Fractals*, 34(1):87–103, 2007.

[10] T. O. Kwok and L. Ling. On convergence of a least-squares Kansa's method for the modified Helmholtz equations. *Adv. Appl. Math. Mech.*, 1(3):367–382, 2009.

[11] T. A. M. Langlands and B. I. Henry. The accuracy and stability of an implicit solution method for the fractional diffusion equation. *J. Comput. Phys.*, 205(2):719–736, 2005.

[12] C.-F. Lee, L. Ling, and R. Schaback. On convergent numerical algorithms for unsymmetric collocation. *Adv. Comput. Math.*, 30(4):339–354, 2009.

[13] L. Ling, R. Opfer, and R. Schaback. Results on meshless collocation techniques. *Eng. Anal. Bound. Elem.*, 30(4):247–253, April 2006.

[14] L. Ling and R. Schaback. Stable and convergent unsymmetric meshless collocation methods. *SIAM J. Numer. Anal.*, 46(3):1097–1115, 2008.

[15] L. Ling and R. Schaback. An improved subspace selection algorithm for meshless collocation methods. To appear in Int. J. Numer. Methods Eng., 2009.

[16] F. Liu, P. Zhuang, V. Anh, and I. Turner. A fractional-order implicit difference approximation for the space-time fractional diffusion equation. *ANZIAM J.*, 47((C)):C48–C68, 2005.

[17] R. Metzler and J. Klafter. Boundary value problems for fractional diffusion equations. *Phys. A*, 278(1-2):107–125, 2000.

[18] R. Metzler and J. Klafter. The random walk's guide to anomalous diffusion: a fractional dynamics approach. *Phys. Rep.*, 339(1):77, 2000.

[19] Z. Odibat and S. Momani. Approximate solutions for boundary value problems of time-fractional wave equation. *Appl. Math. Comput.*, 181(1):767–774, 2006.

[20] Z. Odibat and S. Momani. Numerical solution of Fokker-Planck equation with space- and time-fractional derivatives. *Physics Letters A*, 369:349–358, 2007.

[21] Z. Odibat and S. Momani. Numerical methods for nonlinear partial differential equations of fractional order. *Appl. Math. Modelling*, 32(1):28–39, 2008.

[22] I. Podlubny. *Fractional differential equations*, volume 198 of *Mathematics in Science and Engineering*. Academic Press Inc., San Diego, CA, 1999.

[23] S. Shen, F. Liu, V. Anh, and I. Turner. Detailed analysis of a conservative difference approximation for the time fractional diffusion equation. *J. Appl. Math. Comput.*, 22(3):1–19, 2006.

[24] Z. Sun and X. Wu. A fully discrete difference scheme for a diffusion-wave system. *Appl. Numer. Math.*, 56(2):193–209, 2006.

[25] P. P. Valkó and J. Abate. Numerical inversion of 2-D Laplace transforms applied to fractional diffusion equations. *Appl. Numer. Math.*, 53(1):73–88, 2005.

[26] S. B. Yuste. Weighted average finite difference methods for fractional diffusion equations. *J. Comput. Phys.*, 216(1):264–274, 2006.

[27] P. Zhuang and F. Liu. Implicit difference approximation for the two-dimensional space-time fractional diffusion equation. *J. Appl. Math. Comput.*, 25(1-2):269–282, 2007.

UTMS

2009–9 Jingzhi Li, Masahiro Yamamoto, and Jun Zou: *Conditional stability and numerical reconstruction of initial temperature.*

2009–10 Taku Ishii and Takayuki Oda: *Calculus of principal series Whittaker functions on* $SL(n, \mathbb{R})$.

2009–11 Atsushi Nitanda: *The growth of the Nevanlinna proximity function.*

2009–12 Paola Loreti and Daniela Sforza: *Reachability problems for a class of integro-differential equations.*

2009–13 Masahiro Yamamoto: *Carleman estimates for parabolic equations and applications.*

2009–14 Seiji Nishioka: *Decomposable extensions of difference fields.*

2009–15 Shigeo Kusuoka: *Gaussian K-Scheme.*

2009–16 Shinichiroh Matsuo and Masaki Tsukamoto: *Instanton approximation, periodic ASD connections, and mean dimension.*

2009–17 Pietro Corvaja and Junjiro Noguchi: *A new unicity theorem and Erdös' problem for polarized semi-abelian varieties.*

2009–18 Hitoshi Kitada: *Asymptotically outgoing and incoming spaces and quantum scattering.*

2009–19 V. G. Romanov and M. Yamamoto : *Recovering a Lamé Kernel in a viscoelastic equation by a single boundary measurement.*

2009–20 Hermann Brunner, Leevan Ling and Masahiro Yamamoto: *Numerical simulations of two-dimensional fractional subdiffusion problems.*

The Graduate School of Mathematical Sciences was established in the University of Tokyo in April, 1992. Formerly there were two departments of mathematics in the University of Tokyo: one in the Faculty of Science and the other in the College of Arts and Sciences. All faculty members of these two departments have moved to the new graduate school, as well as several members of the Department of Pure and Applied Sciences in the College of Arts and Sciences. In January, 1993, the preprint series of the former two departments of mathematics were unified as the Preprint Series of the Graduate School of Mathematical Sciences, The University of Tokyo. For the information about the preprint series, please write to the preprint series office.

ADDRESS:
Graduate School of Mathematical Sciences, The University of Tokyo
3–8–1 Komaba Meguro-ku, Tokyo 153-8914, JAPAN
TEL +81-3-5465-7001 FAX +81-3-5465-7012